Optical Methods for Detection of Very Small Vibrations and Design of a Laser Diode System Using Optical Feedback.

Diploma Work
Jonas Sandsten

ABB Corporate Research
and
Lund Institute of Technology
Department of Atomic Physics

Supervisors
Mats Ekberg
Sven-Göran Petterson

Lund Reports of Atomic Physics LRAP 163
Västerås June 1994

Abstract

The aim of this work is to measure very small vibrations. Coherent light is used and its properties are investigated. First, the theory of interferometry and speckles are dealt with. The speckles, often seen as optical noise, are here regarded as vibration information carriers.
Secondly, an active interferometer, based on a V-channel double heterostructure laser diode of Fabry-Perot type, is designed and tested. The frequency of the coherent light emitted from the laser diode is controlled by the injection current. Interference, inside the laser diode, between the emitted light and the scattered light from the vibrating surface give rise to intensity fluctuations. This is optical feedback used in a constructive way. The principles and limitations of an optical feedback interferometer are discussed. Furthermore, design of the electronic circuits that amplify the fluctuating signal and drive the laser diode is presented.

Contents

Chapter 1

Introduction

In advanced metrology in science and industry, coherent light has become very useful [1,2]. Lasers emit coherent light and with the progress in solid state physics it is now possible to make robust, compact and reliable laser diodes [3]. The diodes are inexpensive and easy to work with.
In this diploma work I have done a survey of the scientific literature in search for a strategy to miniaturize a heterodyne Michelson interferometer [4] used as a vibrometer. This vibrometer measures partial discharges generated in isolators. The partial discharge gives rise to an acoustic wave that propagates through the isolator and can be measured on the surface. The acoustic waves have a small amplitude (nm range) and a frequency of less than 10^6 Hz. It will be possible to do preventive diagnostics on high voltage devices without shutting down the power stations if these waves can be measured during operation.
Chapter 2 describes speckle interferometry, one approach of measuring acoustic waves on a surface [5]. Coherent light incident on a surface interferes with the reflected light from the surface and in that way a speckle pattern is seen [6]. The speckle size and position carry information about the surface's motion and roughness. A conclusion from Chapter 2 is that the existing charge coupled devices up to date have not the spatial resolution and readout speed needed to measure the acoustic waves.
I found another strategy, which appears to be more promising than speckle interferometry and bulk optics miniaturization and even outperformed integrated optics. The strategy involves coherent detection with a laser diode, in which the frequency-shifted back scatter light from the vibrating target is coherently mixed with the source light to produce intensity modulation [7]. With the laser diode as both emitter and detector (together with the built-in photo diode) one obtains an extremely sensitive device, with a modulation depth which ordinary homodyne interferometers cannot compete with. Since the back scatter modulation interferometer involves only one lens this is an advantage in mechanically unstable measurement sites. This strategy is described in Chapter 3.
The design of the active interferometer is described in Chapter 4 and the experimental results in Chapter 5.

Chapter 2

Interferometry and Speckles

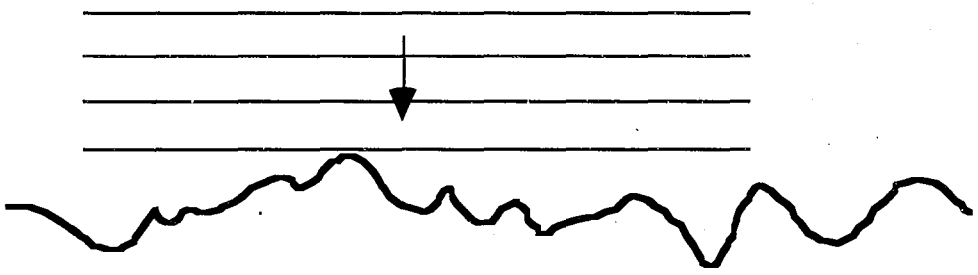

Figure 2.1 Surface with incident coherent wave front.

If a surface is illuminated with coherent light, interference within the reflected light will show up. This is true if the surface is optically rough, that means the roughness must be equal to or greater than one wavelength. The reflected waves travel different distances to the observer. A random interference pattern (superposition of waves) is seen. This phenomenon is called a speckle pattern.

An idea I got was that if the surface vibrates, the speckle phase and intensity should alter. By measuring position and intensity of the speckle pattern it would then be possible to gain information about the surface and its vibration. This idea is already explored and with a set-up as in Figure 2.2 on the next side, a few obvious advantages exist. The entire surface of an object can be illuminated and if there are vibration modes they show up. Another advantage is that sampling the interference pictures makes it possible to process them in a computer after the measurement. A Fourier transform will give what frequencies the vibration modes are oscillating at.

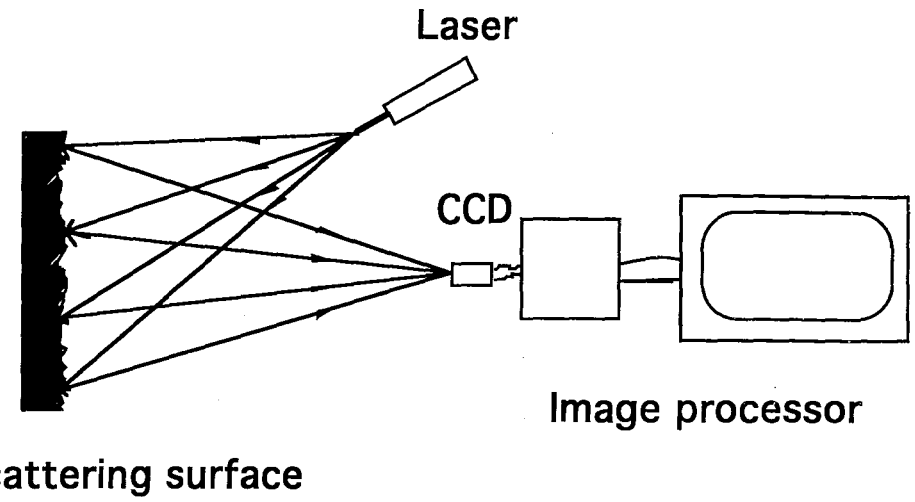

Figure 2.2 Electronic Speckle Pattern Interferometer

The set up in Figure 2.2 is simple and can be done compact. After literature studies I arrived at systems that are commercially available [8-12]. Unfortunately their performance is restricted by some factors, where two important factors are the detector's readout speed and resolution. Because of rapidly evolving Solid State Technology, it is interesting to look for the theoretical limitations of such a system.

2.1 Michelson interferometer (speckle version)

The principle of this instrument is shown in Figure 2.3 [13,14]. A plane wave is split into two paths. In one of the paths there is a reference mirror and in the other path we have the object that we want to measure the displacement of.

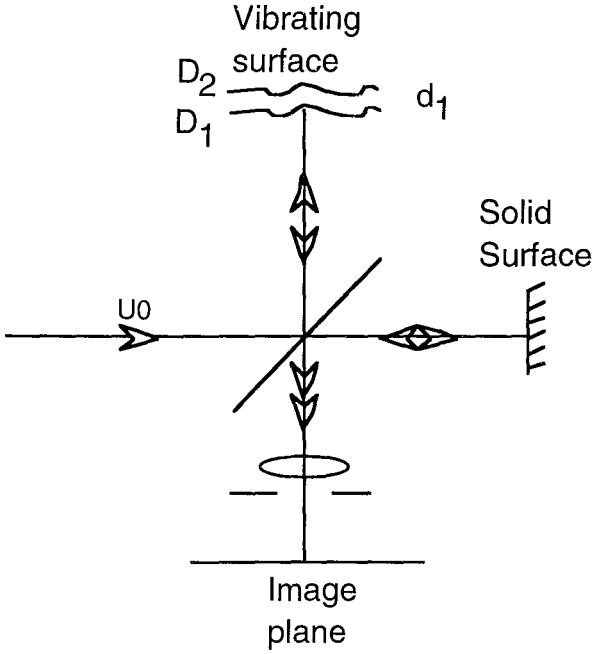

Figure 2.3 Michelson interferometer

The vibrating object will scatter the wave front with a varying phase and the solid reference mirror will scatter the other wave front with constant phase. Besides, the roughness of the surface creates speckles. This means that the object beam have a varying phase due to the vibration and added to that a randomly varying phase due to the roughness of the surface.
The reference beam is modeled as

$$U_1 = u_1 e^{i\psi_1} \tag{2.1}$$

and the object beam is modeled as

$$U_2 = u_2 e^{i\psi_2}. \tag{2.2}$$

At interference the total complex amplitude becomes

$$U_T = u_1 e^{i\psi_1} + u_2 e^{i\psi_2}. \tag{2.3}$$

The intensity is

$$I = UU^* = u_1^2 + u_2^2 + u_1 u_2 \left[e^{i(\psi_1 - \psi_2)} + e^{-i(\psi_1 - \psi_2)} \right] \tag{2.4}$$

that rewritten with Euler´s formula

$$\cos(x) = \frac{1}{2}\left(e^{ix} + e^{-ix}\right) \tag{2.5}$$

is

$$I = u_1^2 + u_2^2 + 2\, u_1 u_2 \cos(\psi_1 - \psi_2) \tag{2.6}$$

or

$$I = I_1 + I_2 + 2\sqrt{I_1 I_2}\cos(\psi_1 - \psi_2). \tag{2.7}$$

When the surface is displaced a distance d_1 parallel to the surface normal, the phase is changed compared to the reference beam.

The phase is changed from 0 to 2π radians for every wavelength that the surface moves. This causes a phase change of

$$\Delta\Phi(d_1) = 2 \cdot 2\pi \cdot \frac{d_1}{\lambda} \tag{2.8}$$

and a new intensity,

$$\hat{I} = I_1 + I_2 + 2\sqrt{I_1 I_2}\cos\left(\psi + \Delta\Phi(d_1)\right) \tag{2.9}$$

arises where $\psi = \psi_1 - \psi_2$. This gives one intensity pattern I in the position D1 and another $\hat{I}$ in D2.

How are these speckle patterns correlated ?
A few conclusions are :

— The intensity is sensitive to amplitude noise in u_1 and u_2.

— When $\Delta\Phi(d_1) = 2\pi n$ the intensities are the same, $I = \hat{I}$ and the speckle patterns are correlated.

— When $\Delta\Phi(d_1) = (2n+1)\pi$ there is no correlation.

This means that the resulting speckle pattern varies in intensity and spatial location due to the vibration. The calculation of correlation is made in [6].

2.2 Speckle theory

To gain knowledge about the nature of speckles (intensity, shape and size) we need a thorough mathematical analysis. But first some assumptions that are made here:

A complex representation $\alpha_k e^{j\phi_k}$ carries information about the phase, ϕ_k and the reflection, α_k from a scattering point on the surface. The phase represents the position (depth) of the scattering point. All of the scattering points contribute to the speckle pattern or speckle resultant

$$\bar{a} = ae^{j\theta} = \frac{1}{\sqrt{N}} \sum_{k=1}^{N} \alpha_k e^{j\phi_k} . \tag{2.10}$$

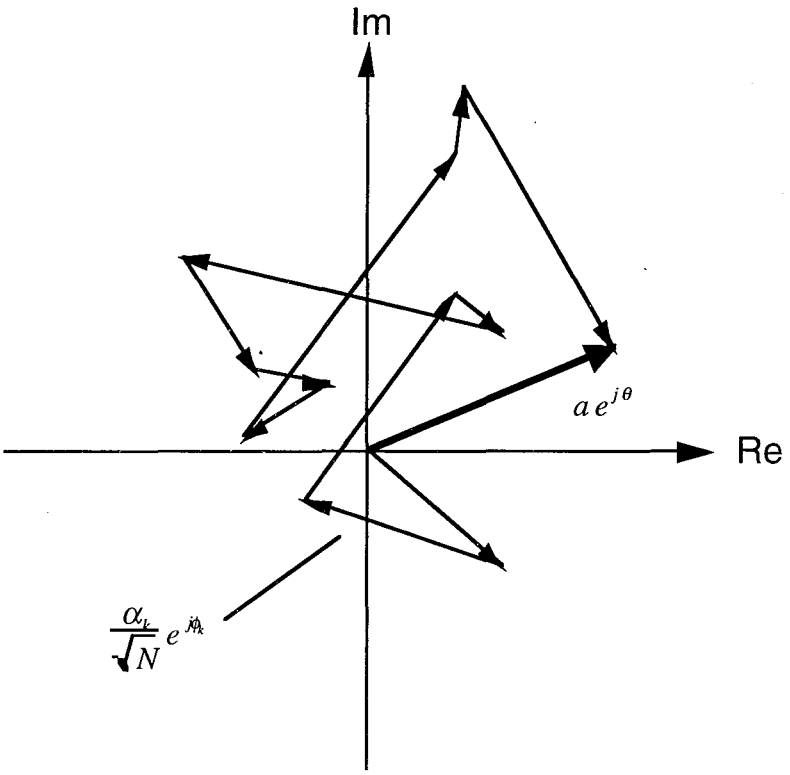

Figure 2.4 Speckle resultant, made of 11 scattering points.

However, the following statistical assumptions must now be made for a continuing analysis :

1. The amplitude and phase of each scattering point are statistically independent of every other scattering point.

2. The stochastic variables α_k are identical for all k, with mean $\bar{\alpha}_k$ and moment $\overline{\alpha^2}$.

3. The phases ϕ_k are uniformly distributed over the interval $-\pi, \pi$.

The speckle resultant $ae^{j\theta}$ is now split in one real and one imaginary part. The real part r is defined as

$$r = \mathrm{Re}\{ ae^{j\theta} \} = \frac{1}{\sqrt{N}} \sum_{k=1}^{N} \alpha_k \cos\phi_k \tag{2.11}$$

and the imaginary part i is defined as

$$i = \mathrm{Im}\{ ae^{j\theta} \} = \frac{1}{\sqrt{N}} \sum_{k=1}^{N} \alpha_k \sin\phi_k . \tag{2.12}$$

Both r and i have an approximately Gaussian distribution when N is large (due to the Central Limit Theorem). With mean and variance it is now possible to derive the probability density function. The mean of r and i is

$$\begin{aligned} \bar{r} &= \frac{1}{\sqrt{N}} \sum_{k=1}^{N} \overline{\alpha_k \cos\phi_k} = \frac{1}{\sqrt{N}} \sum_{k=1}^{N} \overline{\alpha_k}\,\overline{\cos\phi_k} = \sqrt{N}\,\bar{\alpha}\,\overline{\cos\phi} \\ \bar{i} &= \frac{1}{\sqrt{N}} \sum_{k=1}^{N} \overline{\alpha_k \sin\phi_k} = \frac{1}{\sqrt{N}} \sum_{k=1}^{N} \overline{\alpha_k}\,\overline{\sin\phi_k} = \sqrt{N}\,\bar{\alpha}\,\overline{\sin\phi} \ . \end{aligned} \tag{2.13}$$

Because of equally distributed phases over the interval $-\pi, \pi$, is

$$\overline{\cos\phi} = \overline{\sin\phi} = 0 \ \Rightarrow \quad \bar{r} = \bar{i} = 0 . \tag{2.14}$$

The variances σ_r^2 and σ_i^2, $\left(\sigma^2 = \overline{r^2} - \bar{r}^2\right)$ are needed and that is why the moment is calculated as

$$\begin{aligned} \overline{r^2} &= \frac{1}{N} \sum_{k=1}^{N} \sum_{n=1}^{N} \overline{\alpha_k \alpha_n}\,\overline{\cos\phi_k \cos\phi_n} \\ \overline{i^2} &= \frac{1}{N} \sum_{k=1}^{N} \sum_{n=1}^{N} \overline{\alpha_k \alpha_n}\,\overline{\sin\phi_k \sin\phi_n} \end{aligned} \tag{2.15}$$

$$\overline{\cos\phi_k \cos\phi_k} = \overline{\sin\phi_k \sin\phi_k} = \begin{cases} 0 & k \neq n \\ \dfrac{1}{2} & k = n \end{cases}$$

$$\Rightarrow \quad \overline{r^2} = \overline{i^2} = \frac{\overline{\alpha^2}}{2} = \sigma^2 . \tag{2.16}$$

This completes the Gaussian probability density function:

$$P_{RI}(r,i) = \frac{1}{2\pi\sigma^2} e^{\left(-\frac{r^2+i^2}{2\sigma^2}\right)} . \tag{2.17}$$

Some conclusions at this stage are that $\bar{a}$, the resultant of the scattering points is a circular, complex and Gaussian stochastic variable. If the phases are not

equally distributed over the interval $-\pi,\pi$, then $\bar{a}$ becomes elliptic [6]. Using the fact that we have circular symmetry it is convenient to transform the coordinates to polar ones.

$$\begin{aligned} a &= \sqrt{r^2+i^2} \\ \theta &= \arctan\frac{i}{r} \end{aligned} \qquad \text{which gives} \qquad \begin{aligned} r &= a\cos\theta \\ i &= a\sin\theta \end{aligned} \quad . \tag{2.18}$$

The functional determinant is written

$$\left\| \begin{matrix} \frac{\partial r}{\partial a} & \frac{\partial r}{\partial \theta} \\ \frac{\partial i}{\partial a} & \frac{\partial i}{\partial \theta} \end{matrix} \right\| = \left\| \begin{matrix} \cos\theta & -a\sin\theta \\ \sin\theta & a\cos\theta \end{matrix} \right\| = a.$$

This means that the probability density function is

$$P_{A\theta}(a,\theta) = P_{RI}(r = a\cos\theta, i = a\sin\theta)\cdot a \tag{2.19}$$

which gives

$$P_{A\theta}(a,\theta) = \frac{a}{2\pi\sigma^2} e^{-\frac{a^2}{2\sigma^2}} \qquad -\pi < \theta \le \pi\,,\, a > 0. \tag{2.20}$$

Integrating from -π to π gives

$$P_A(a) = \int_{-\pi}^{\pi} P_{A\theta}(a,\theta)d\theta = \frac{a}{\sigma^2} e^{-\frac{a^2}{2\sigma^2}} \qquad a > 0, \tag{2.21}$$

which is the Rayleigh distribution with mean $\bar{a} = \sqrt{\frac{\pi}{2}}\,\sigma$.

With the Rayleigh distribution it is now possible to continue the analysis of the nature of speckles.
The intensity $I = A^2 \Rightarrow A = \sqrt{I}$ and Eq. (2.21) becomes

$$P_I(I) = P_A\left(A = \sqrt{I}\right)\left|\frac{dA}{dI}\right| = \frac{\sqrt{I}}{\sigma^2} e^{-\frac{I}{2\sigma^2}} \frac{1}{2\sqrt{I}} = \frac{1}{2\sigma^2} e^{-\frac{I}{2\sigma^2}} \qquad I \ge 0, \tag{2.22}$$

where a more compact writing is

$$P_I(I) = \frac{1}{\bar{I}} e^{-\frac{I}{\bar{I}}} \quad I \ge 0. \tag{2.23}$$

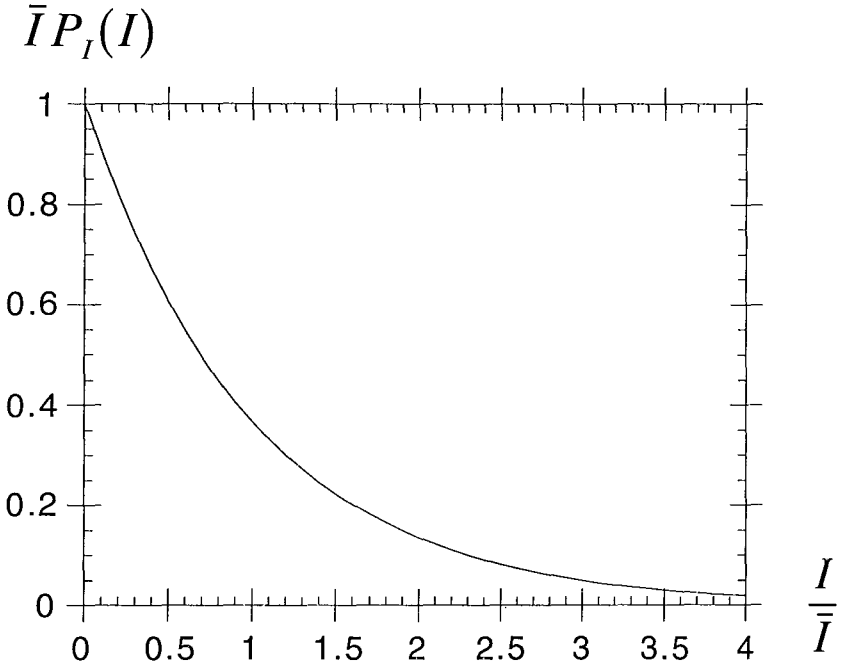

Figure 2.5 The most probable intensity is black.

$\bar{I}$ is the mean value of the speckle pattern intensity, averaged over a large number of scattering points in the reflected field. The standard deviation is equal to the mean value with Rayleigh distribution function, $\sigma_I = \bar{I} = 2\sigma^2$, which in turn means that the contrast, $c = \sigma_I / \bar{I} = 1$ [2]. In those cases the speckles are regarded as noise the have an annoyingly high contrast.

2.3 The mean of the speckle size

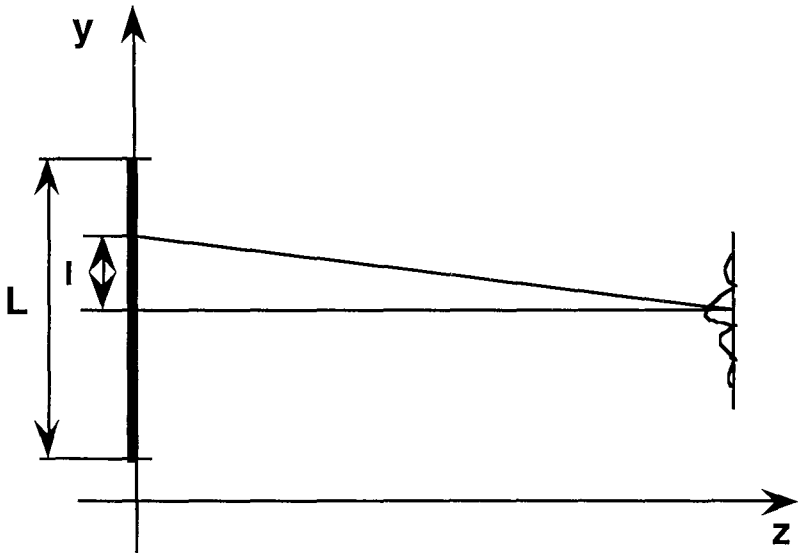

Figure 2.6 Objective speckles, formed on the image plane, made from a surface´s scattering points at z=0 with length L.

The surface in y-direction is illuminated with coherent light, without an imaging lens we obtain objective speckles in the image plane. These speckles form fringes with the spatial frequency

$$f = \frac{l}{\lambda z} . \tag{2.24}$$

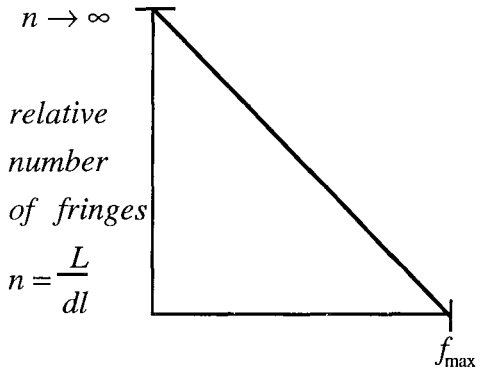

Figure 2.7 The fringe spatial frequency distribution.

Using Figure 2.7 makes it possible to write the mean of the fringe spatial frequency. The number of paired fringes per frequency unit divided by the total number of fringes per frequency unit is

$$\frac{\int_0^L \frac{l}{\lambda z}(L-l)dl}{\int_0^L (L-l)dl} = \frac{1}{3}\frac{L}{\lambda z}. \tag{2.25}$$

The mean of the fringe spatial frequency is

$$\overline{f} = \frac{1}{3} f_{max} = \frac{1}{3}\frac{L}{\lambda z} \tag{2.26}$$

and the intensity in an ordinary two-beam fringe pattern from [1] is

$$I = 1 + \cos\left(\frac{Ly}{\lambda z}\right). \tag{2.27}$$

The speckle pattern vary in a similar way. The conclusion is that the speckles twinkle due to a vibration in the z-direction.

2.4 Example of ESPI-Electronic Speckle Pattern Interferometer

The starting point is a Michelson interferometer where the fringes are given at a phase difference, $\Delta\Phi(d_1) = 2 \cdot 2\pi \cdot \frac{d_1}{\lambda}$ as shown earlier.

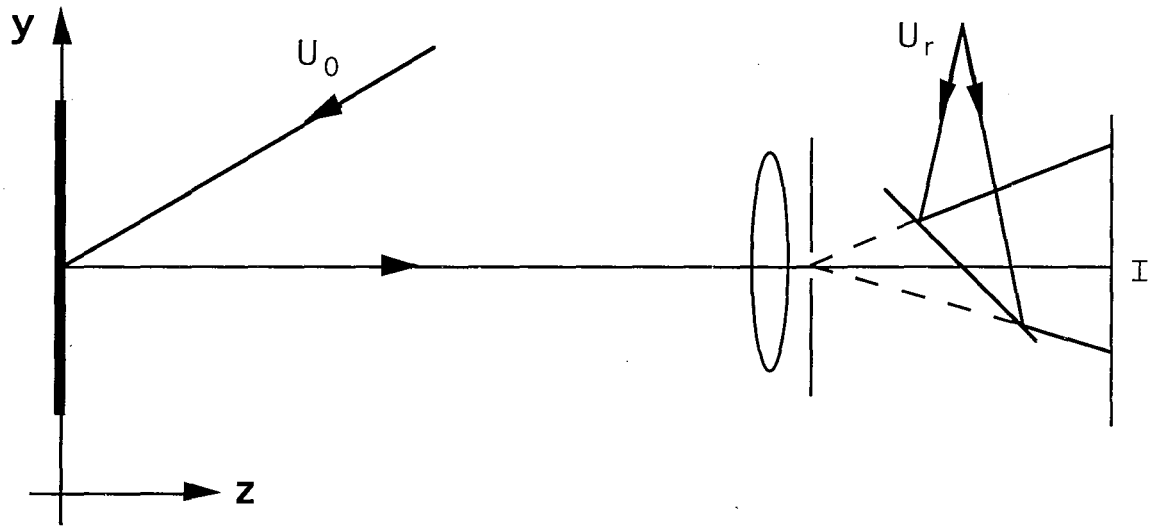

Figure 2.8 ESPI-Electronic Speckle Pattern Interferometer

In the Figure 2.8 above a so called "smooth in-line reference wave front" is shown, which gives one of the most sensitive ESPI methods. The reference wave front interferes with the object wave front and fringes appear. If the object moves, we have a phase difference

$$\Delta\phi = \frac{2\pi(1+\cos\theta_1)d_1}{\lambda} \tag{2.28}$$

which means that the fringes twinkles, due to the displacement in z-direction.

2.5 Limitations of ESPI

The most important feature in speckle interferometry is the fact that it is possible to illuminate a large surface to see if there exist modes of oscillation. That is why a charge coupled device detector (CCD) is used in these systems. A normal CCD has data as follows : 20 μm distance between the light sensitive spots. This gives 1/20 = 50 periods/mm as the highest spatial frequency. The distance between two positions of the reflector can be calculated if the phase difference is set to 2π as

$$\Delta\phi = 2\pi = \frac{2\pi(1+\cos\theta_1)d_1}{\lambda} \Rightarrow d_1 = \frac{1}{2}\lambda \,. \tag{2.29}$$

My conclusions from this chapter is:

- An estimate of the least detectable displacement is a half wavelength.

- The CCD readout speed 25 Hz is a bandwidth limit if a European TV-system is used. The fastest CCD, known to me, is not fast enough in our application.

Our goal is to be able to measure sub-nm displacements at a frequency of 1 MHz. These limitations made me search for another concept and design a system based on an active interferometer. Chapter 3 and 4 describes the new concept.

Chapter 3

Active Interferometer Displacement Follower

This chapter deals with active multiple beam interferometers [15-19].
Chapter 2 gave us mathematical tools to understand two-beam interferometry and speckles. In a passive interferometer the object beam is compared with a stable reference beam. The intensity and frequency stability is critical. However, if the reference beam is set to a fixed condition, like a fixed intensity or phase, and the interference signal is fed back to the reference beam, we have an active interferometer.
Historically almost all interferometers where made with helium-neon gas lasers. A laser diode is similar to the helium-neon laser in that the emitted radiation is highly monochromatic and produces a highly directional beam of light. However, the laser diode differs from a gas laser in that it is small (L_D = 250μm) and is easily modulated simply by modulating the injection current.

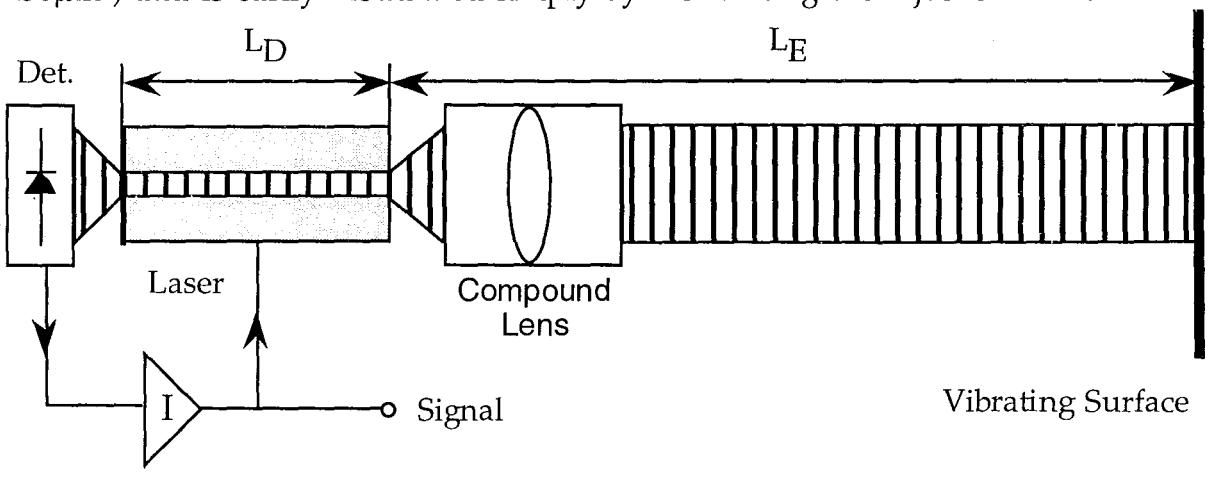

Figure 3.1 Small-displacements follower set to a fixed phase condition. The frequency and output power of the coherent light emitted from the laser diode is controlled by the injection current. Interference, inside the laser diode, between the emitted light and the scattered light from the surface give rise to intensity fluctuations.

3.1 Operation principle

The operational principle of the active interferometer we have designed is readily understood by studying Figure 3.1. When injection current enters the p-n junction a population inversion is induced. Photons are stimulated by spontaneous emission and those photons that are reflected back into the gain medium from the crystal facets will give rise to lasing. The critical inversion of the gain medium and the mirror reflectances give the lasing condition

$$R_1 R_2 e^{(2\sigma(N_2-N_1)L_D)} = 1, \tag{3.1}$$

where R_1 is the back facet reflectivity, R_2 is the front facet reflectivity, σ is the absorption cross section, $N_2 - N_1$ is the critical inversion and L_D is the length of the active medium. A coherent wave front is then sent from the laser diode onto a surface. The surface vibrates and scatters a small portion of the light back to the laser diode. The beams interfere inside the laser diode (Fabry-Perot interference) and intensity fluctuations can be registered with a sensitive photo diode. To understand why we get intensity fluctuations at the photo diode we need a simple model of an optical resonator [14].

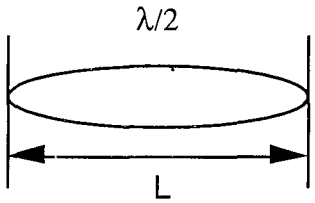

Figure 3.2 Optical resonator with its standing wave.

A laser diode is an optical resonator made of different semiconductor materials and structures. We have used a Fabry-Perot cavity laser diode with V-channel double-heterostructure substrate in this work. It is gallium-arsenide based and emit a single mode in the near-infrared region. In the resonator described by Figure 3.2, longitudinal modes can exist between the mirrors. To have a standing wave in the resonator it is necessary that

$$L = m\frac{\lambda}{2\bar{n}}, \tag{3.2}$$

where m is a longitudinal mode number, λ is the mode wavelength and $\bar{n}$ is the refractive index of the wave guide. If a back scattered wave enters the cavity it will interfere with the lasing mode. The effect on the laser power of this interference is described in Figure 3.3 on the next side.

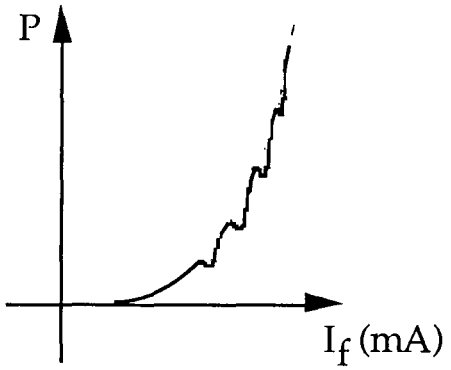

Figure 3.3 Intensity fluctuations in the laser diode.

Small undulations because of destructive interference is seen, where the laser wavelength has shifted from one longitudinal mode to another, this corresponds to a vibration amplitude of $\lambda/2$ between two undulations. By setting the amplifier to give a certain bias current varied with a current that follows the vibration this yield the movement. In the approach of reference [19] the output intensity P is compared with a reference intensity, P_0 at the undulation. The interferometer output is a function of the phase delay, δ and it is written

$$P = P(\delta). \tag{3.3}$$

The feedback current

$$I = A(P - P_0) \tag{3.4}$$

where A is the gain in the feedback loop. The injection current controls the laser frequency and can be modeled as

$$f = f_0 + \chi I, \tag{3.5}$$

where f_0 is a constant corresponding to P_0 and χ is a constant explained in Figure 3.4. As in Chapter 2 Eq. (2.8) the frequency change affects the phase as

$$\delta = \frac{4\pi f D}{c}, \tag{3.6}$$

where D is the optical path difference and f is the laser frequency.

Working with the equations (3.4-6) above will give

$$P = P(\delta, D) = \left(P_0 - \frac{f_0}{\chi A}\right) + \left(\frac{c}{4\pi D \chi A}\right) \cdot \delta. \tag{3.7}$$

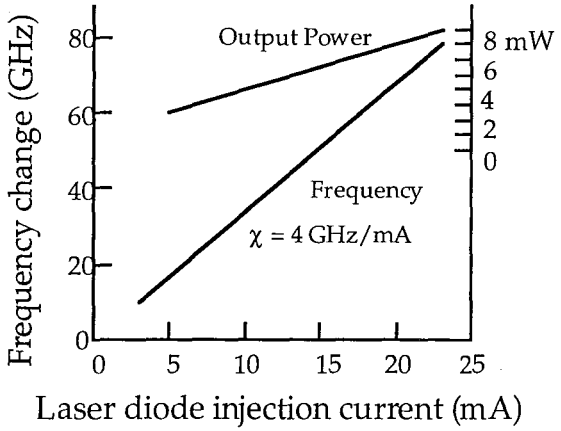

Figure 3.4 Illustration on how a laser diode responds to a change in injection current. This figure comes from [19].

Stationary states of the feedback loop in Figure 3.1 are given by the solutions to Eq. (3.2) and Eq. (3.6). This means that the phase dependence must be specified. In a two-beam interferometer the intensity is

$$P = a + b\cos(\delta), \tag{3.8}$$

but in the case of multiple-beam interferometer the Fabry-Perot model is useful [19] :

$$P = P_1 R = P_1\left(\frac{F\sin^2\delta + G}{1 + F\sin^2\delta}\right), \tag{3.9}$$

where $F = \dfrac{4r_2r_3}{(1-r_2r_3)^2}$ and $G = \left(\dfrac{r_2 - r_3}{1 - r_2r_3}\right)^2$.

r_2 and r_3 are the amplitude reflectivity of the reflector and the laser facet respectively.

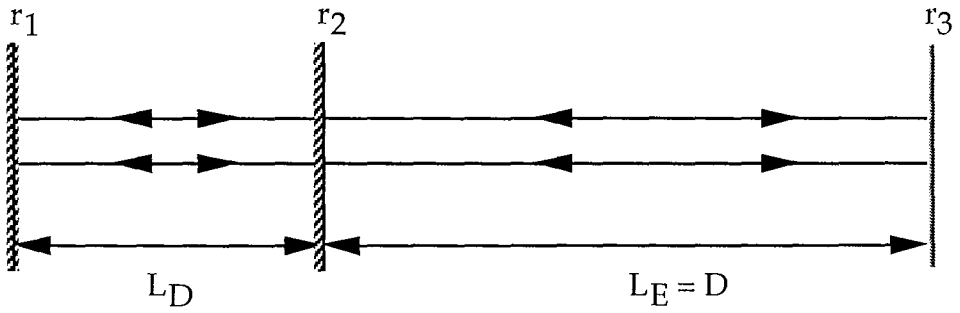

Figure 3.5 Reflectivity and lengths in a compound cavity model.

In Figure 3.5 L_D is the laser cavity length and L_E is the external cavity length. L_E is the same as the distance to the surface. If r_3 is small (which is the case for a typical high-voltage device), R in Eq. (3.9) becomes

In Figure 3.5 L_D is the laser cavity length and L_E is the external cavity length. L_E is the same as the distance to the surface. If r_3 is small (which is the case for a typical high-voltage device), R in equation 3.9 becomes

$$R = (1-G)F\sin^2\delta + G \tag{3.10}$$

A change in

$$\delta = \frac{4\pi f D}{c}$$

causes a change in the Q value of the resonator and hence in its output power. The undulations are obvious.
What is the change in wavelength between two longitudinal modes in an optical resonator? The external cavity modes are separated as

$$\Delta\omega_E = \frac{\pi c}{L_E} \quad \Rightarrow \quad \Delta\lambda_E = \frac{\lambda^2}{2L_E} \tag{3.11}$$

and the allowed longitudinal modes in the laser cavity are separated by

$$\Delta\lambda_D = \frac{\lambda^2}{2\bar{n}L_D}, \tag{3.12}$$

here $\bar{n}$=3.5 as it is the refractive index of GaAlAs, L_D=250 μm is the laser cavity length and L_E=93 mm, taken as an example from the experiments in Chapter 5. This makes $\Delta\lambda_E$=0.0033 nm and $\Delta\lambda_D$=0.35 nm. Hence, several of the external cavity modes are available under the laser gain curve. The laser will oscillate at the most favorable for lasing, near the allowed mode, that is an integral multiple of the modes in the external cavity. The external cavity sets the phase more precise compared to the free running laser diode and this makes the coherence length L_c increase.

$$L_c \approx \frac{c}{\bar{n}\Delta f} = \frac{\lambda^2}{\bar{n}\Delta\lambda}, \tag{3.13}$$

where $\Delta\lambda$ is the spectral bandwidth.

3.2 Temperature effects

The effects of temperature fluctuations in a laser diode are a frequency shift and mode hopping. A drive current increase, shifts the laser emission to a slightly longer wavelength by increasing the laser cavity's temperature and refractive index. More power is dissipated as heat in the crystal and the effective cavity length is increased. This affects the separation, $\Delta\lambda_D$, between

two modes in the longitudinal direction, which is the difference in wavelength corresponding to m and m+1.

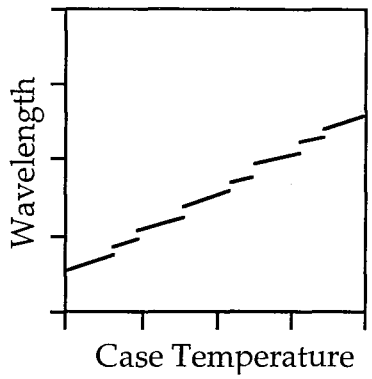

Figure 3.6 Schematic illustration of modehopping with increasing temperature.

Within an oscillation mode, m, the rate of change due to a change in temperature is [19] :

$$\frac{\partial \omega_m}{\partial T} = \frac{\partial \omega_m}{\partial \lambda_m}\frac{\partial \lambda_m}{\partial T} = \frac{-2\pi c}{\lambda_m^2}\frac{\partial \lambda_m}{\partial T}. \tag{3.15}$$

3.3 The scattered light

The scattered light from a surface depends on irradiance, wavefront appearance and reflectivity. If the incident light is monochromatic and the surface is optically rough, as defined in Chapter 2, even speckles becomes important. In a first approximation it is enough to look at the mean value of the speckles.
From a diffusely scattering surface (such a surface is a model of a high-voltage surface) every point scatters the light in all directions. The irradiance obeys

$$I \propto \frac{1}{r^2}, \tag{3.16}$$

where r is the distance from the surface to the observer. More specifically

$$I(r) = \rho\frac{A}{r^2}I_0 \quad \left[W/m^2\right], \tag{3.17}$$

where ρ is a surface constant, A is the diffuse area, r is the distance and I_0 is the incident irradiance. According to [5] a mat white surface has $\rho = 8\cdot 10^{-8} \quad m^2\,mm^{-2}$. The reflectance required for feedback, defined as the light power that enters the laser diode divided by the totally emitted power is now estimated, with typical values for the laser diodes used. $I_0 = 5\,mW$ and the

beam area is $7.5 \times 2.5 = 18.75\ mm^2$ which is the same as the diffuse area. The system front aperture collects light at a distance of one meter and the diameter is 50 mm. This gives a reflectance of 1.8%. The corresponding modulation depth [18] is then fairly small but this is in favor for the stability of the laser diode. In fact if the reflectance becomes more than a few tens of a percent [16] we have not the situation where a single mode inside the laser interferes with the incoming light. The optimum relative external reflectance is 0.02% according to [19]. For strong feedback there exists a coherence collapse region where many modes compete in a chaotic way [20].

The conclusion from the above is that the light from a diffusely scattering surface is sufficient to interfere with the lasing mode.

Chapter 4

Design of an active interferometer

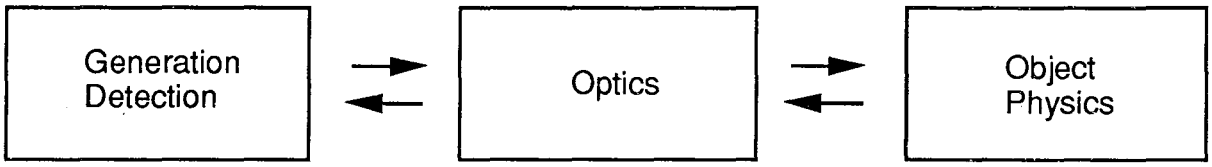

Figure 4.1 Design structure

4.1 Instrument requirements

The instrument should be able to measure partial discharges without making any contact with the isolator surface. Several hundred kilovolts may be present at the measurement site. High electromagnetic fields must not disturb the instrument. Mechanical vibrations <1000 Hz due to the line frequency 50 Hz overtones must be filtered out. The isolator surface scatters the light diffusely which means that the instrument must be very sensitive.

Some facts :

- The object is acoustic transient waves.
- Measurement distance : >0.5 meter
- Amplitude : 1μm down to sub-nm
- Frequency interval : 100 kHz - 1 MHz

4.2 Design

4.2.1 Optics

The optical components are used to collimate, focus and prolong the coherence length of the beam from the laser diode. Besides, gathering light from the reflecting surface should be done. Inside the interferometer, lens surfaces

should be anti-reflection coated, otherwise internal interference may disturb the instrument. A simple lens is to prefer over a complex multi-element system due to less surfaces. That was why we thought of using a GRIN, (GRadient INdex) lens at first. In a gradient index lens the refractive index varies parabolically as a function of radius. As a result of this index variation, a ray incident on the front surface follows a sinusoidal path along the rod lens. The period of this path is called the "Pitch". With a 0.23 Pitch the lens behaves as a collimator.

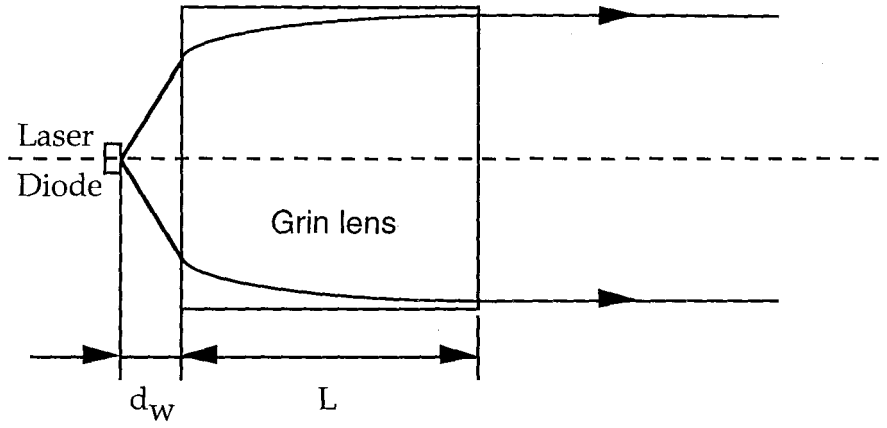

Figure 4.2 GRIN lens collimating laser output

If the entrance and exit surfaces are curved and anti-reflection coated we have almost no feedback from the surfaces. With the maximum acceptance angle for the lens, $2\theta = 55° \Rightarrow N.A. = n \cdot \sin\theta = 0.46$. A laser diode that emits its light in two angles due to the rectangular opening have $\theta_1 = 30°$, $\theta_2 = 10°$ $\Rightarrow N.A. \approx 0.5$. This is more than the numerical aperture of the lens. Some of the light would not be collected. Another problem with the GRIN lens is the working distance, d_W. For the case with a pitch of 0.23 at 830 nm, d_W is 0.21 mm. This is a problem because the laser chip is mounted inside a housing at a distance of 0.93 mm from the outer side of the protective glass.

A solution to the problems above is to use a complex lens system. We chose a Melles Griot lens 06GLC001 with aberration corrections, a N.A. = 0.615 and a working distance, f_W = 0.78 mm as our collimating lens.

The reflectance of the external cavity mirror is calculated as follows. The photon lifetime, τ_c in the external cavity is

$$\tau_c = \frac{L_E}{\gamma c} = \frac{1}{2\pi\Delta\upsilon_c}, \qquad (4.1)$$

where γ is the logarithmic losses [14], L_E is the cavity length and $\Delta\upsilon_c$ is the linewidth of the resonator.
For a measurement distance of 1.5 m the coherence length, L_c should be at least 3 m. This give us the required linewidth as

$$\Delta v_c = \frac{c}{L_c} = 100\ MHz \tag{4.2}$$

The logarithmic losses is written

$$\gamma = \gamma_i + \frac{\gamma_1 + \gamma_2}{2}, \tag{4.3}$$

where γ_i is the internal losses, which here includes the diffraction losses plus the coupling loss to the laser diode aperture. $\gamma_i \approx 2\%$ in this estimate.

$$\gamma_1 = -\ln(1 - T_1) \tag{4.4}$$

is the loss at the back facet of the laser diode and

$$\gamma_2 = -\ln(1 - T_E) \tag{4.5}$$

is the loss at the external mirror. With values from the laser diode we have used, shown in figure 4.3 and an external cavity length of 0.24 m, the reflectance of the external mirror, R_E should be ≈40%.

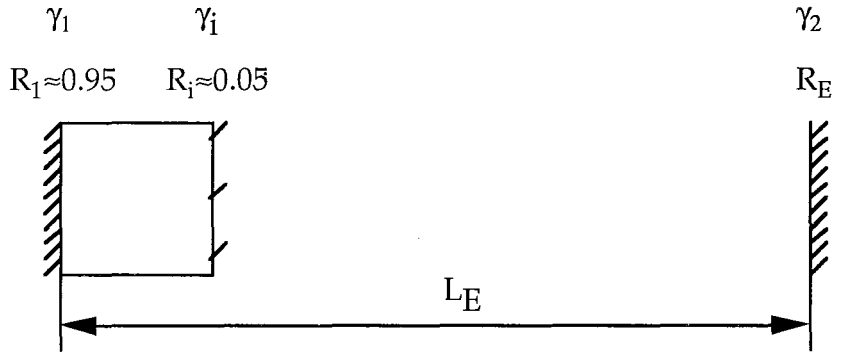

Figure 4.3 External mirror reflectance estimate.

To make the signal to noise ratio better it is noticeable that this should be done with optics before working with signal processing. An interference filter that acts as a bandpass filter with its center wavelength matching the laser wavelength will enlarge S/N ratio. Stray light is screened away.

4.2.2 Optoelectronics

Under this header the technical aspects of the laser diode and the photo diode will be dealt with. The laser diode we have used is a Sharp LT027MF [21]. The diode emit infrared radiation at 780 nm with a power of 10 mW. To be able to aim the instrument beam at a chosen spot on the object surface, the light should preferably be visible. Alternatively the use of a visible indicator beam could position the measurement beam. Another important consideration is the irradiance of the spot. The scattered light must not be harmful to the eyes.

One of the reasons to use an infrared laser diode is the stability of the single longitudinal mode and as mentioned earlier its Fabry-Perot cavity.
Besides, these laser diodes have facet reflectances well suited for interference inside the gain wave guide.

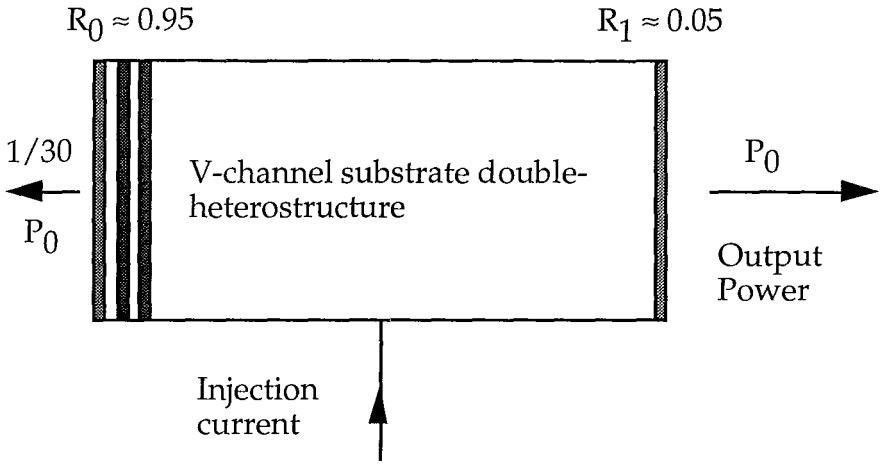

Figure 4.3 Laser cavity and its reflectances, typical for the used laser diode.

The reflectance of the front mirror is deliberately made low by anti-reflection coating, which makes $R_1 \approx 5\%$. This makes it possible for the reflected beam to enter the cavity and interfere with the lasing mode.
The theoretical coherence length of a Fabry-Perot laser is

$$L_c = \frac{c}{\Delta f} \tag{4.6}$$

where c is the speed of light and Δf is the laser diodes spectral linewidth. Normally the coherence length of a laser diode is a few mm. However, according to [18] the coherence length of their laser diode system is 4-6 meters. The half of this length would then be the longest measurement distance. Their coherence length might be explained in the following way. As the scattering surface acts as an external cavity the practical coherence length is prolonged because of increased cavity photon lifetime, as shown is Chapter 3.

In the detection scheme, the photo diode and the laser diode work together. As discussed before in this chapter a lasing mode interferes with the back scattered wave inside the laser diode. The fluctuations that appear are then registered with a built-in photo diode. This specialized pin-diode is very fast and optimized for the laser wavelength in use. The photo diode is mounted behind the laser diode and approximately 1/30 of the lasing mode illuminate the photo diode. Because of the small intensity fluctuations that we want to lock on and a high "background" level, the lasing mode, it is necessary to use extremely sensitive preamplifiers. But before discussing the features of these amplifiers we will look into the physics of the pin-photo diode [22].

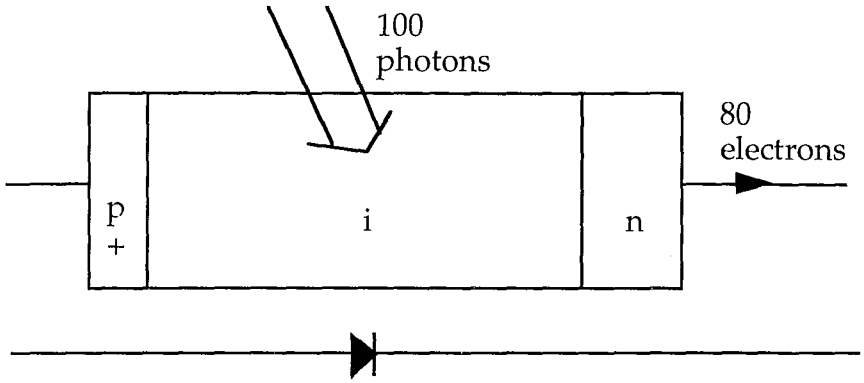

Figure 4.3 The pin-photo diode with a quantum efficiency of 0.8.

The depletion region is enlarged with an intrinsic layer between the pn-junction. Herein the photons are captured. If one photon is matching or exceeding the band-gap of the semiconductor its energy will release an electron (and a hole) which in turn is swept away by the electric field. The remaining energy goes to phonon scattering processes. The generated signal current is

$$i_s = \frac{\eta e P}{h \upsilon}, \tag{4.7}$$

where η is the quantum efficiency, e is the electron charge, P is the power of the incident light, h is the Planck constant and υ is the frequency of the light. Together with dark current i_0 , the voltage V, Boltzman's constant k_B and the temperature T we write the current-voltage response of the diode as

$$i = i_0\left(e^{\frac{eV}{k_B T}} - 1\right) - i_s. \tag{4.8}$$

The frequency response of the photo diode depends on how it is operated. In the photo voltaic mode, the carriers are swept away by the junction built-in voltage. This makes a sensitive circuit. In the photo conductive mode an external voltage is applied and the carriers are swept away much faster. This makes the diode frequency response faster. In Figure 4.4 this process is equivalent to changing the capacitance C.

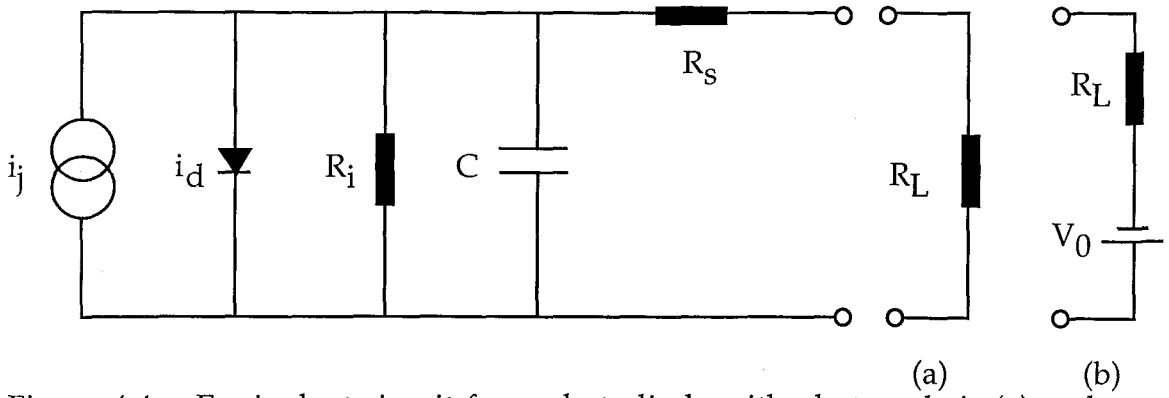

Figure 4.4 Equivalent circuit for a photodiode with photo voltaic (a) and photo conductive (b) detection.

In general $R_i >> R_L >> R_S$ [22], so that the cut-off frequency f_c is written

$$f_c = \frac{1}{2\pi R_L C}. \tag{4.9}$$

In this work the photo voltaic mode is used, the photo diode and the laser diode are wired together with a common pin and this means that the photo diode cannot be reverse biased with an external voltage.

4.2.3 Electronics

The desired instrument should function with battery supply and besides that, transients from the 220 V line will not disturb the instrument with a battery solution. The power supply is designed with ±24 Volts batteries that are voltage regulated to give +5, ±15 Volts. Because of extremely narrow linewidths in the structures of laser diodes, handling requires precautions. Electrostatic discharge (a few hundred volts is enough) destroys the laser diodes.

Driving the laser diode is done with an automatic current control circuit. This driver has a slow starter function to raise the current slowly. Current control can be made internally with a potentiometer or externally with a function generator. The Automatic Current Control (ACC) circuit is found in Appendix A.

The preamplifier circuit is also found in Appendix A. It is a current to voltage converter (transimpedance amplifier) where the current from the photo diode is amplified, $-i_s R$. The feedback resistor R should be as large as possible (consistent with bandwidth requirements) to minimize noise. This seems paradoxical because the thermal noise voltage increases as :

$$u = \sqrt{4 k_B T \Delta f R} \tag{4.10}$$

where k_B is Boltzman's constant, T is the temperature (°K), Δf the system bandwidth (Hz), R is the feedback resistor and u is the noise voltage ($V_{rms.}$). However, the transimpedance gain (signal) increases as :

$$u = -i_s R \tag{4.11}$$

where i_s is the signal current. Altogether this makes the signal-to-noise ratio improve by $\sqrt{R}$.
The design was delicate due to the influence of stray capacitance and the large amplification feedback resistors.

Chapter 5

Experiment evaluation

Laser diodes are all individuals. That means the supplier gives data within broad tolerances. To find out how our LT027MF [21] laser diode and photo diode worked, the first measurements was optical output versus injection current. Figure 5.1 shows this relation.

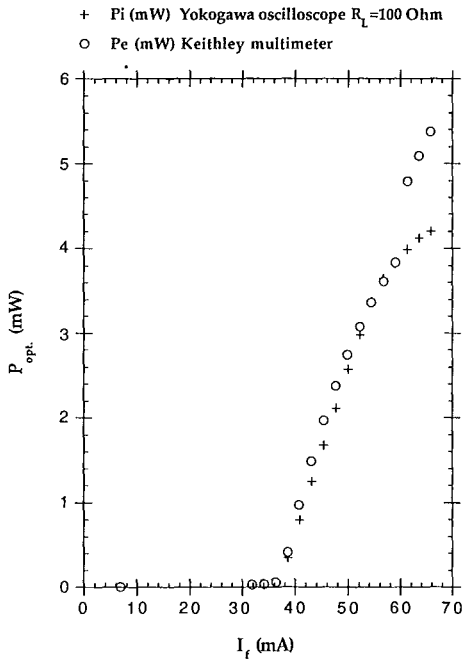

Figure 5.1 Output power from the laser diode LT027MF measured with the internal photo diode in photo voltaic mode. Compared with the external photo diode connected directly to a Keithley multimeter. The kink at 4 mW is due to switching R_L in the multimeter.

From this measurement it is seen that the photo diode's internal impedance must be matched to the following preamplifier. The laser threshold current is 36 mA, but it increases with temperature. Temperature stabilization should be done when we experiment with the laser diode, but for the active

interferometer it is not obviously necessary because of the steady state situation. Remember, the injection current increases the wavelength through increased temperature. In this work we have not stabilized the temperature.

An extremely accurate coupling of the backscattered light into the 1×3 μm aperture of the laser diode is needed. In the second experiment, where the laser threshold was supposed to be lowered when light in phase with the lasing mode enters the cavity, another effect was observed. The Figure 5.2 shows the effect.

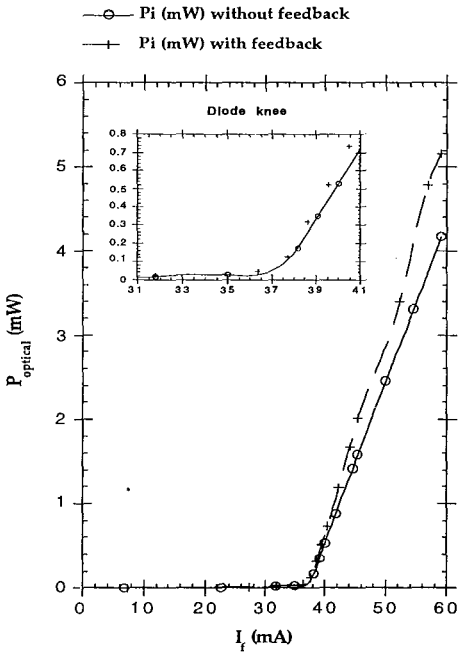

Figure 5.2 Laser threshold with and without badly coupled external feedback. The external cavity length, L_E=5 cm and the optical density is 0.5.

The effect seen is that when a wide focus spot illuminates part of the aperture and part of the photo diode mounted behind the laser diode the intensity is higher but the threshold current is not lowered. To avoid this problem nm-positioning both in the direction of the optical axis and in the laser aperture plane is needed. nm-positioning was not at hand so it was tricky to couple the backscattered light into the aperture.

The **highlights** of this diploma work are now presented.
When a precise coupling of the feedback light was accomplished the undulations appeared. Figures 5.3-5 on page 32 shows the undulations. In case that the external cavity length is equal to an integral multiple of the laser diode cavity length, the feedback light comes in phase and that makes constructive interference with the oscillating mode. In the experiment the external cavity length is fixed and the injection current that controls the frequency is varied.

The set-up is shown in Figure 5.6 on page 32. A fixed neutral density filter is used as reflector and it has a optical density of 0.04, which is the same as a transmittance of 91.2%. Less than 8.8% is reflected. The losses are absorbance in the filter and resonator logarithmic losses in the external cavity plus coupling losses to the laser aperture. The external cavity length is ≈93 mm.
The Figures 5.3-4 shows a voltage ramp that is fed to the ACC circuit from a function generator. Its frequency is 94 Hz. Over this ramp is the intensity seen and it is measured with the internal photo diode. It takes approximately 10 seconds for the laser diode to move from an undulation peak when a fixed injection current is set and that means that the temperature is at a steady state because of the 94 Hz ramp modulation of current. Figure 5.5 should have the same underlying curvature as figure 3.3 but it has not, this is due to the ACC response. In Appendix A the driver electronics is fed with the function generator voltage at the point where the potentiometer is coupled. Then the operational amplifier is in a feedback loop which has a RC-like response to its input. At the beginning of the ramp the photo diode picks up spontaneous emitted light. Lasing is marked with an arrow in Figure 5.3. This figure is enlarged in the Figures 5.4 and 5.5.

The distance between two undulations is $\lambda/2$ and the signal to noise ratio, $S/N \approx 6$. This might be used as a resolution estimate of the displacement follower. $\lambda = 780$ nm $\Rightarrow$ resolution=65 nm. The bandwidth in use is 20 MHz and with the required bandwidth of 1 MHz the S/N ratio will be improved and so the resolution.

A concluding remark:
The amplification in the feedback loop controls the bandwidth and thereby the resolution of the displacement follower. Parts of 65 nm can be resolved according to the discussion above.

5.1 Prototype suggestion

After the amplification of the interference signal it should be fed back to the laser diode to change its frequency and thereby follow the vibration. The requirements of such a circuit is a well defined dynamic range and a function that detects in what direction the vibration is at. The dynamic range of the circuit is in conflict with its signal to noise ratio, but an upper limit of the bandwidth is 1 MHz. Direction detection can be done by differentiating the signal. The dynamic range, 18 undulations multiplied with $\lambda/2$ could be made longer if one adds a digital counter that counts the number of mode jumps that the displacement follower goes through and resets the injection current to a lower/higher bias current depending on if the vibrating surface is moving away or towards the instrument.

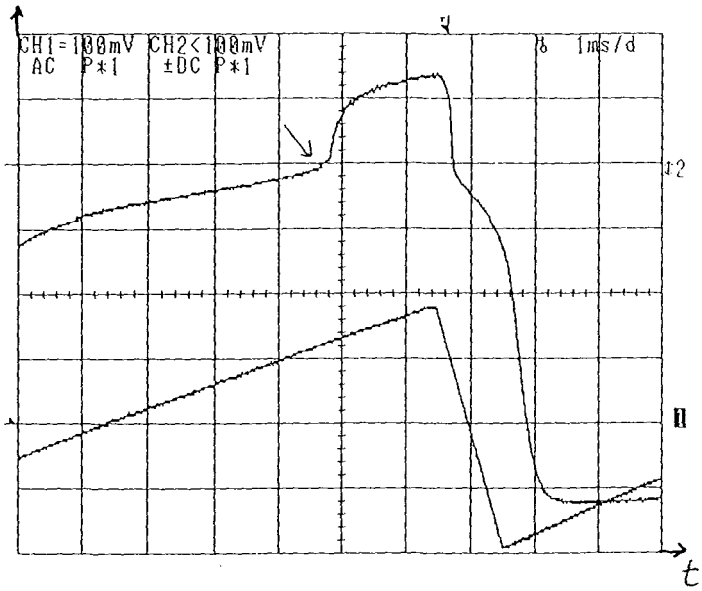

Figure 5.3 Current ramp and photo diode voltage.

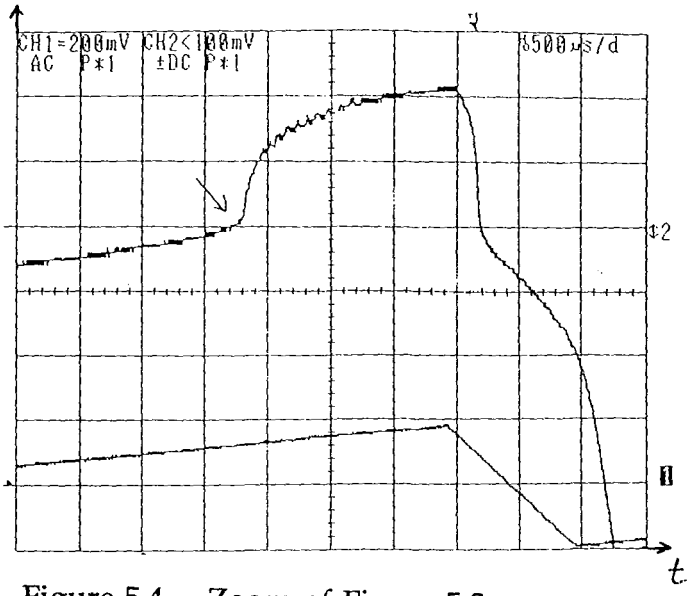

Figure 5.4 Zoom of Figure 5.3.

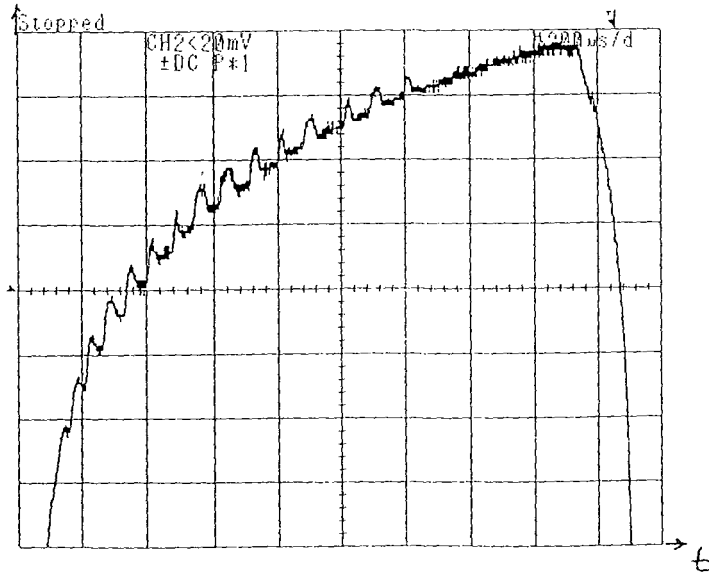

Figure 5.5 Undulations for a fixed external cavity length.

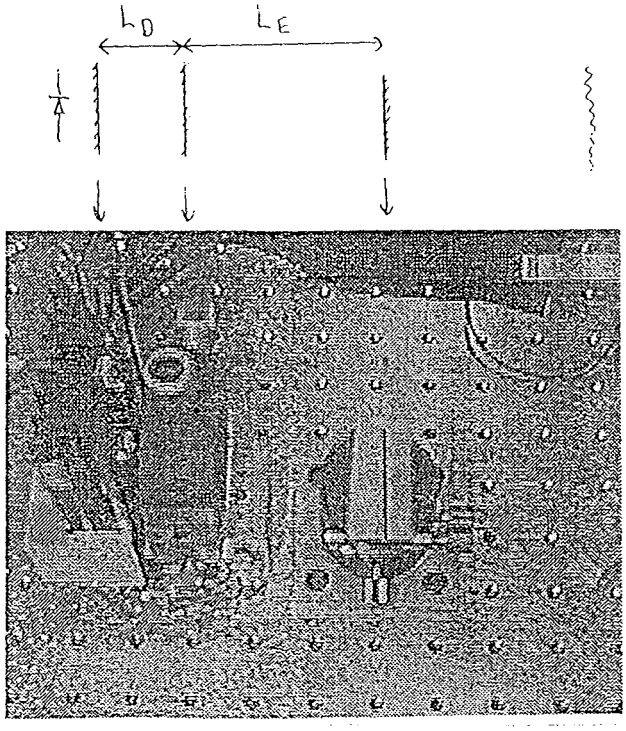

Figure 5.6 The set-up consists of a laser diode, a collimating lens and a positioner for the external cavity mirror.

Chapter 6

Conclusions

A summary of the work is done here :

Chapter 2

A few conclusions are :

— The intensity is sensitive to amplitude noise in u_1 and u_2.

— When $\Delta\Phi(d_1) = 2\pi n$ the intensities are the same, $I = \hat{I}$ and the speckle patterns are correlated.

— When $\Delta\Phi(d_1) = (2n+1)\pi$ there is no correlation.

This means that the resulting speckle pattern is varying in intensity and spatial location on the CCD detector.

Page 6

The most important feature in speckle interferometry is the fact that it is possible to illuminate a large surface to see if there exist modes of oscillation. That is why a charge coupled device detector (CCD) is used in these systems. A normal CCD has data as follows : 20 μm distance between the light sensitive spots. This gives 1/20 = 50 periods/mm as the highest spatial frequency. The distance between two positions of the reflector can be calculated if the phase difference is set to 2π as

$$\Delta\phi = 2\pi = \frac{2\pi(1+\cos\theta_1)d_1}{\lambda} \quad \Rightarrow \; d_1 = \frac{1}{2}\lambda \; . \tag{2.29}$$

- This will be a measure of the least detectable displacement.

- The CCD readout speed 25 Hz is a bandwidth limit if a European TV-system is used. The fastest CCD, known to me, is not fast enough in our application. **Page 12**

Chapter 3

The conclusion from "3.3 The scattered light" is that the light from a diffusely scattering isolator is sufficient to interfere with the lasing mode inside the active interferometer. **Page 19**

Chapter 4

By using a large resistance, R in the feedback of the operational amplifier the signal-to-noise ratio improves by $\sqrt{R}$. **Page 26**

Chapter 5

The amplification in the feedback loop controls the bandwidth and thereby the resolution of the displacement follower. Parts of 65 nm can be resolved. **Page 30**

Acknowledgements

The author thank Mats Ekberg and Tord Bengtsson ABB Corporate Research for their valuable advice and support during the diploma work. Thanks also to Sven-Göran Pettersson and Peter Kauranen at the department of Atomic Physics in Lund for support and material. A special thank to Mats Leijon ABB Corporate Research for believing in and financing the diploma work.

Bibliography

[1] S. Borgström, S-G. Pettersson
Optisk Teknik KF-Sigma Lund (1992)

[2] S. Svanberg
Atomic and Molecular Spectroscopy Springer-Verlag (1991)

[3] S.M. Sze
Semiconductor Devices Physics and Technology
John Wiley & Sons (1985)

[4] P. Bårmann
Development of a Heterodyne Laser Interferometer for Very Small High Frequency Displacements Detection Lund report of atomic physics LRAP 137 Dep. of Atomic Physics LIT (1992)

[5] C.M. Vest
Holographic Interferometry
John Wiley & Sons

[6] J.W. Goodman
Statistical Optics New York Wiley cop. (1985)

[7] R. Lang and K. Kobayashi
External Optical Feedback Effects on Semiconductor Injection Laser Properties
IEEE Journal of Quantum Electronics vol. **16** (1980)

[8] Y. Ohtsuka
Dynamic measurements of small displacements by laser interferometry Trans Inst M C vol. **4** (1982)

[9] Editor W.P. Jüptner
Industrial Applications of Holographic Speckle Measuring Technics
Proceedings of the SPIE vol. **1508** (1991)

[10] F.M. Santoyo, M.C. Shellabear, J.R. Tyrer
Four cases of engineering vibration studies using pulsed ESPI
Proceedings of the SPIE vol. **1508** (1991)

[11] O.J. Løkberg et. al
Computerized vibration analysis of hot objects
Proceedings of the SPIE vol. **1508** (1991)

[12] J.R. Tyrer
Critical review of recent developments in electronic speckle pattern interferometry
Proceedings of the SPIE vol. **604** (1986)

[13] E. Hecht and A. Zajac
Optics Addison-Wesley (1974)

[14] S. Borgström
Laserfysik KF-Sigma Lund (1992)

[15] J.H. Churnside
Laser doppler velocimetry by modulating a CO_2 laser with backscattered light
Applied Optics vol. **23** (1984)

[16] J. Kato and I. Yamaguchi
A multi-dimensional displacement sensor using the optical feedback of laser diodes
Proceedings of the SPIE vol. **1553** (1991)

[17] P.J. de Groot, G.M. Gallatin, S.H. Macomber
Ranging and velocimetry signal generation in a backscatter - modulated laser diode
Applied Optics vol. **27** (1988)

[18] P.J. de Groot and G.M. Gallatin
Backscatter-modulation velocimetry with an external cavity laser diode
Optics Letters vol. **14** (1989)

[19] T. Yoshino et. al
Laser diode feedback interferometer for stabilization and displacement measurements
Applied Optics vol. **26** (1987)

[20] J. Mørk, B. Tromborg,J. Mark, V.Velichansky
Instabilities in a laser diode with strong optical feedback
Proceedings of the SPIE vol. **1837** (1992)

[21] Sharp Corp.
Laser Diode User's Manual
Ref. no. HT509D Japan (1988)

[22] E. Udd
Fiber Optic Sensors Chapter 4
John Wiley & Sons (1991)

Appendix A

Slow Starter and Driver

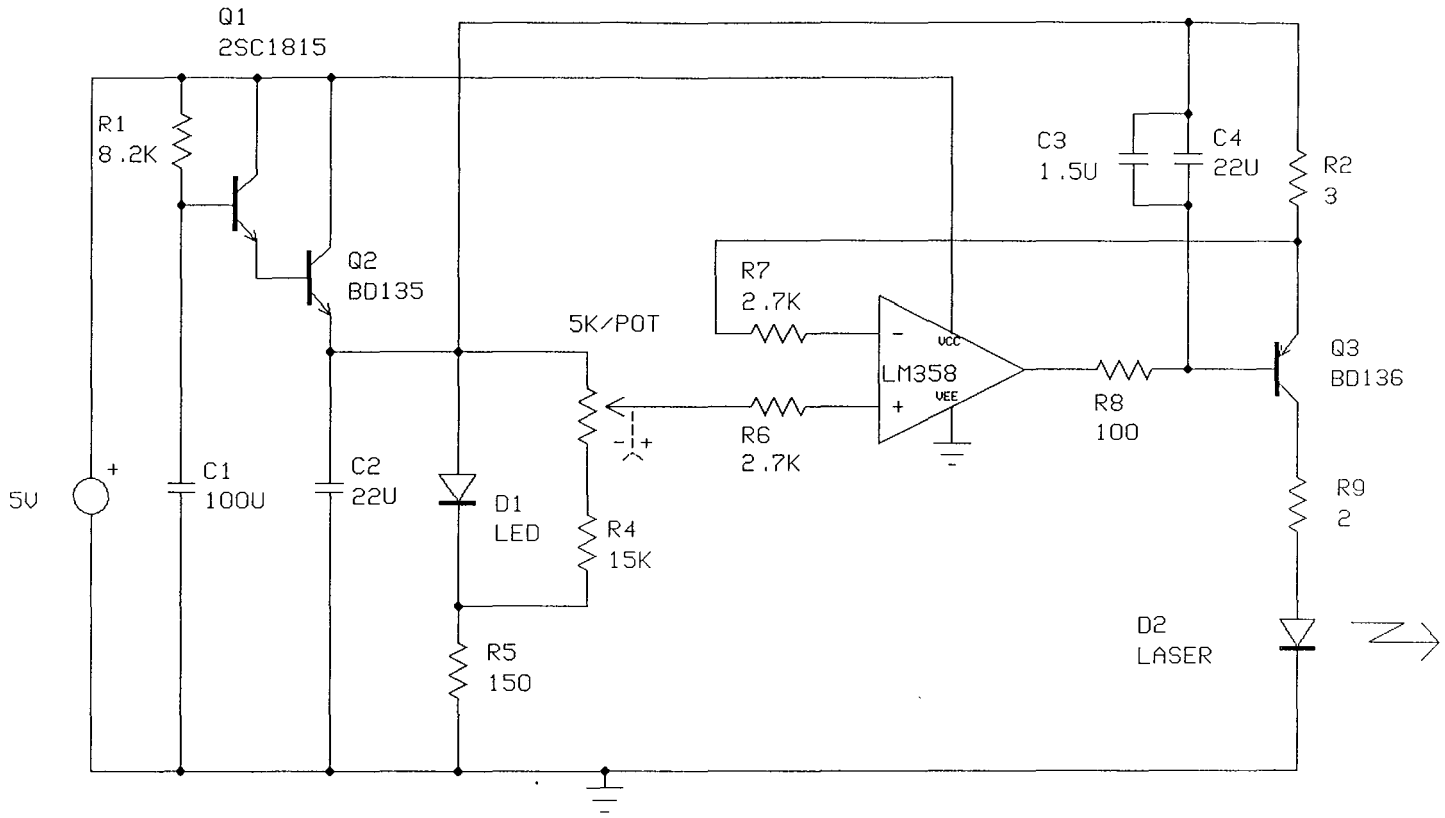

PIN Diode Preamplifier

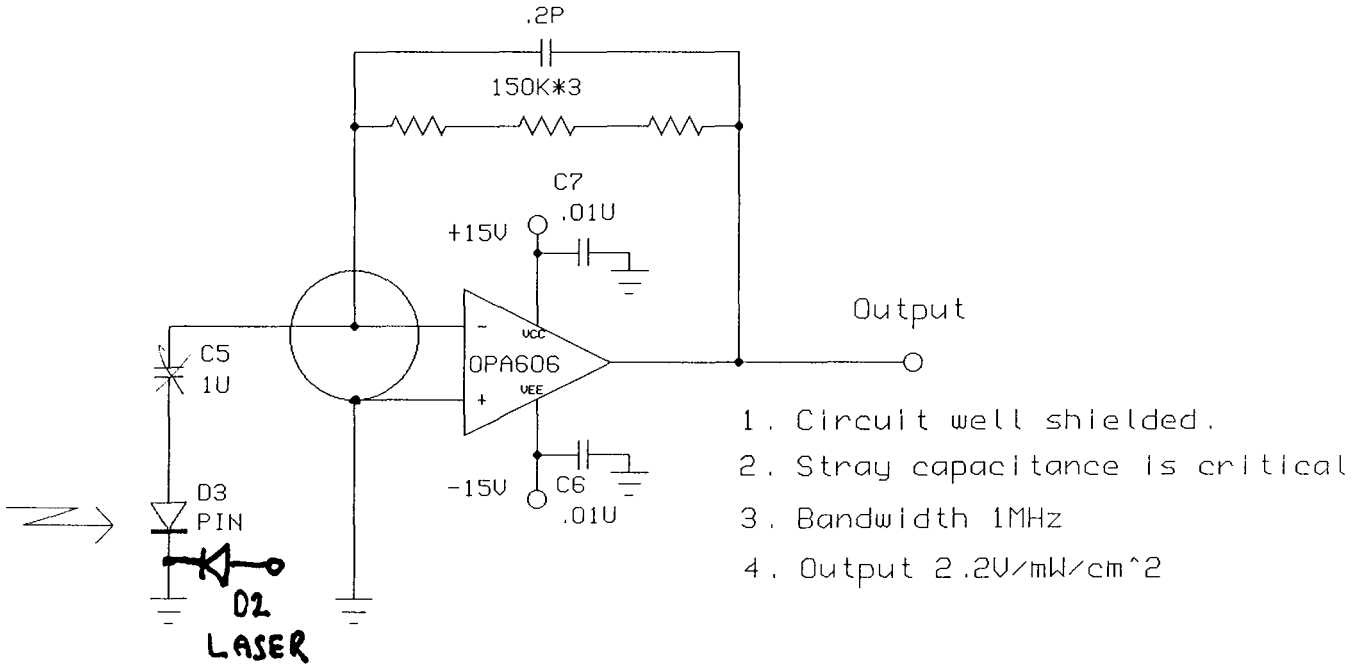

1. Circuit well shielded.
2. Stray capacitance is critical
3. Bandwidth 1MHz
4. Output 2.2V/mW/cm^2